Mineralogical Magazine, August 2013, Vol. 77(6), pp. 2811–2823

Joteite, $Ca_2CuAl[AsO_4][AsO_3(OH)]_2(OH)_2{\cdot}5H_2O$, a new arsenate with a sheet structure and unconnected acid arsenate groups

A. R. Kampf[1,*], S. J. Mills[2], R. M. Housley[3], G. R. Rossman[3], B. P. Nash[4], M. Dini[5] and R. A. Jenkins[6]

[1] Mineral Sciences Department, Natural History Museum of Los Angeles County, 900 Exposition Boulevard, Los Angeles, CA 90007, USA
[2] Geosciences, Museum Victoria, GPO Box 666, Melbourne 3001, Australia
[3] Division of Geological and Planetary Sciences, California Institute of Technology, Pasadena, CA 91125, USA
[4] Department of Geology and Geophysics, University of Utah, Salt Lake City, UT 84112, USA
[5] Pasaje San Agustin 4045, La Serena, Chile
[6] 4521 N Via Madre, Tucson, AZ 85749, USA

[*Received 18 Mary 2013; Accepted 11 July 2013; Associate Editor: F. Cámara*]

ABSTRACT

Joteite (IMA2012-091), $Ca_2CuAl[AsO_4][AsO_3(OH)]_2(OH)_2{\cdot}5H_2O$, is a new mineral from the Jote mine, Tierra Amarilla, Copiapó Province, Atacama, Chile. The mineral is a late-stage, low-temperature, secondary mineral occurring with conichalcite, mansfieldite, pharmacoalumite, pharmacosiderite and scorodite in narrow seams and vughs in the oxidized upper portion of a hydrothermal sulfide vein hosted by volcanoclastic rocks. Crystals occur as sky-blue to greenish-blue thin blades, flattened and twinned on {001}, up to ~300 μm in length, and exhibiting the forms {001}, {010}, {1$\bar{1}$0}, {2$\bar{1}$0} and {111}. The blades are commonly intergrown in wheat-sheaf-like bundles, less commonly in sprays, and sometimes aggregated as dense crusts and cavity linings. The mineral is transparent and has a very pale blue streak and vitreous lustre. The Mohs hardness is estimated at 2 to 3, the tenacity is brittle, and the fracture is curved. It has one perfect cleavage on {001}. The calculated density based on the empirical formula is 3.056 g/cm^3. It is optically biaxial (−) with α = 1.634(1), β = 1.644(1), γ = 1.651(1) (white light), $2V_{meas}$ = 78(2)º and $2V_{calc}$ = 79.4º. The mineral exhibits weak dispersion, $r < v$. The optical orientation is $X \approx \mathbf{c}^*$; $Y \approx \mathbf{b}^*$. The pleochroism is Z (greenish blue) > Y (pale greenish blue) > X (colourless). The normalized electron-microprobe analyses (average of 5) provided: CaO 15.70, CuO 11.22, Al_2O_3 8.32, As_2O_5 46.62, H_2O 18.14 (structure), total 100 wt.%. The empirical formula (based on 19 O a.p.f.u.) is: $Ca_{1.98}Cu_{1.00}Al_{1.15}As_{2.87}H_{14.24}O_{19}$. The mineral is slowly soluble in cold, concentrated HCl. Joteite is triclinic, $P\bar{1}$, with the cell parameters: a = 6.0530(2), b = 10.2329(3), c = 12.9112(4) Å, α = 87.572(2), β = 78.480(2), γ = 78.697(2)º, V = 768.40(4) Å^3 and Z = 2. The eight strongest lines in the X-ray powder diffraction pattern are [d_{obs} Å(I)(hkl)]: 12.76(100)(001), 5.009(23)(020), 4.206(26)(120,003,121), 3.92(24)(022,0$\bar{2}$2,$\bar{1}$02), 3.40(25)($\bar{1}$13), 3.233(19)(031,023,123,0$\bar{2}$3), 2.97(132,201) and 2.91(15)($\bar{1}$22,$\bar{1}$13). In the structure of joteite (R_1 = 7.72% for 6003 $F_o > 4\sigma F$), AsO_4 and $AsO_3(OH)$ tetrahedra, AlO_6 octahedra and $Cu^{2+}O_5$ square pyramids share corners to form sheets parallel to {001}. In addition, 7- and 8-coordinate Ca polyhedra link to the periphery of the sheets yielding thick slabs. Between the slabs are unconnected $AsO_3(OH)$ tetrahedra, which link the slabs only via hydrogen bonding. The Raman spectrum shows features consistent with OH and/or H_2O in multiple structural environments. The region between the slabs may host excess Al in place of some As.

* E-mail: akampf@nhm.org
DOI: 10.1180/minmag.2013.077.6.08

Keywords: joteite, new mineral, arsenate, acid arsenate, Raman spectroscopy, crystal structure, Jote mine, Tierra Amarilla, Chile.

Introduction

THE Pampa Larga mining district near the city of Tierra Amarilla in Chile's Copiapó Province is a well known source of rare As-bearing mineral species. The Alacrán mine is the type locality of alacránite, As_8S_9 (Popova *et al*., 1986), the Maria Catalina mine is the type locality for rruffite, $Ca_2Cu(AsO_4)_2{\cdot}2H_2O$ (Yang *et al*., 2011) and the Veta Negra mine yielded remarkable crystals of the mineral miguelromeroite, $Mn_5(AsO_3OH)_2(AsO_4)_2{\cdot}4H_2O$ (Kampf, 2009). These and other past mineral discoveries in the district drew one of the authors (RAJ) to explore the dumps of the Jote mine, which is now no more than a small abandoned adit. The specimens from this 2007 visit yielded the first crystals of the new mineral species described herein. In 2011 and 2012 Arturo Molina collected specimens from within the adit, which provided better crystals of the new species.

The new mineral is named joteite (hou tei ait) for the locality. The new mineral and name have been approved by the Commission on New Minerals, Nomenclature and Classification of the International Mineralogical Association (IMA2012-091). The description of the new mineral was based upon three specimens, which are designated cotype specimens and are deposited in the Natural History Museum of Los Angeles County, 900 Exposition Boulevard, Los Angeles, CA 90007, USA under catalogue numbers 63592, 63593 and 63594. The three cotypes were collected in 2007, 2011 and 2012, respectively.

Occurrence and paragenesis

The mineral occurs at the Jote mine, Pampa Larga district, Tierra Amarilla, Copiapó Province, Atacama Region, Chile. The mineralization occurs in a narrow (20–40 cm wide) hydrothermal vein hosted by volcanoclastic rocks. The occurrence is similar to that of the new mineral rruffite (IMA2009-077; Yang *et al*., 2011) at the Maria Catalina mine. A detailed description of the geology and mineralogy of the area was provided by Parker *et al*. (1963).

The deeper, unoxidized, portion of the vein contains primary and supergene minerals including acanthite, native arsenic, Ag sulfosalts, baryte, calcite, chalcopyrite, domeykite, feldspar, pyrite, quartz, native silver and stibnite. Joteite occurs as a late-stage, low-temperature, secondary mineral in narrow seams and vughs in the oxidized upper portion of the vein. The matrix is an intergrowth of quartz and microcline–albite "microperthite". The microperthite varies from fresh to heavily altered. The more heavily altered areas are impregnated with massive mansfieldite and/or scorodite. Other secondary minerals in direct association with joteite are conichalcite, pharmacoalumite, pharmacosiderite and at least two other new Ca-Cu-Al arsenates (currently under study). Other minerals found in the oxidation zone include ceruleite, chlorargyrite, gartrellite, goudeyite, gypsum, karabibite, koritnigite, krautite, lavendulan, metazeunerite, olivenite, opal, rruffite and zincolivenite.

Physical and optical properties

Crystals occur as blades up to ~300 μm long, but are generally much smaller. The blades are very thin, rarely exceeding 5 μm in thickness. The blades are commonly intergrown in wheat-sheaf-like bundles (Figs 1 and 2) and less commonly in sprays (Fig. 3). Aggregates sometimes form dense crusts and cavity linings. Crystals are flattened on {001}, elongate approximately along [120] and exhibit the forms {001}, {010}, $\{1\bar{1}0\}$, $\{2\bar{1}0\}$ and {111} (Fig. 4). Twinning by reflection on {001} is ubiquitous.

Joteite is sky blue to greenish blue and has a very pale blue streak. Crystals are transparent and have vitreous lustre. Joteite does not fluoresce in long- or short-wave ultraviolet light. The Mohs hardness is estimated to be between 2 and 3 based upon the behaviour of crystals when broken. The

FIG. 1. Wheat-sheaf-like intergrowth of subparallel joteite crystals (~0.15 mm across) with pharmacoalumite.

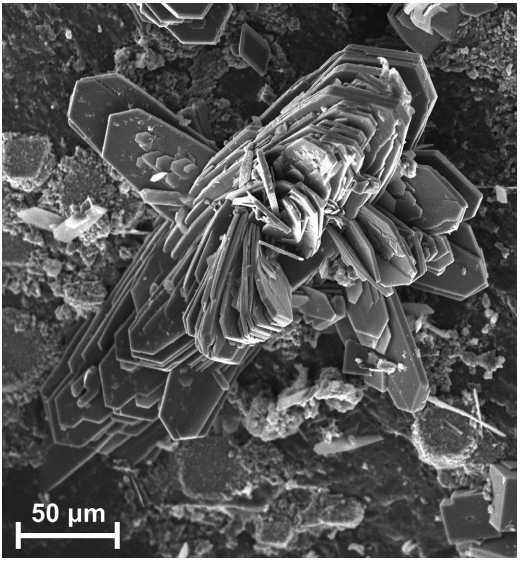

FIG. 2. Stack of divergent blades of joteite forming a wheat-sheaf-like aggregate (SEM image).

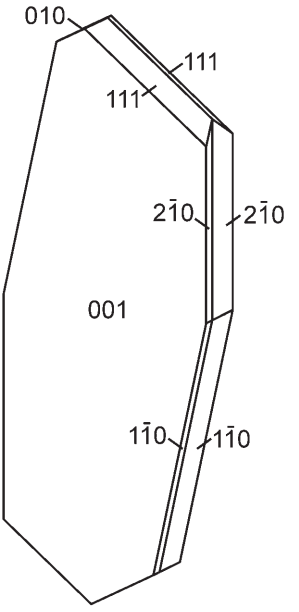

FIG. 4. Crystal drawing of a joteite contact twin on {001} (clinographic projection in non-standard orientation, [120] vertical).

tenacity is brittle and the fracture is curved. Crystals exhibit perfect cleavage on {001}. Attempts to measure the density by sink-float in Clerici solution were unsuccessful because individual crystals proved too difficult to see and larger aggregates contained trapped air. The calculated density based on the empirical formula and the unit cell determined by single-crystal X-ray diffraction is 3.056 g/cm^3. Joteite is slowly soluble in cold, concentrated HCl.

Optically, joteite is biaxial negative, with α = 1.634(1), β = 1.644(1) and γ = 1.651(1), measured in white light. The 2V measured directly by conoscopic observation is 78(2)º. The calculated 2V is 79.4º. The mineral exhibits weak dispersion, $r < v$. The optical orientation is $X \approx \mathbf{c}^*$; $Y \approx \mathbf{b}^*$ and the pleochroism is Z (greenish blue) > Y (pale greenish blue) > X (colourless).

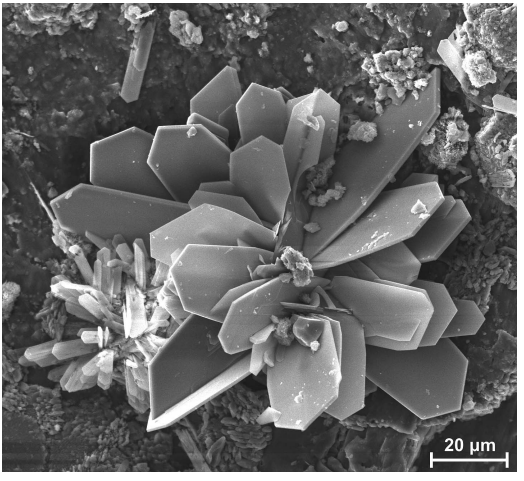

FIG. 3. Spray of joteite blades (SEM image).

Raman spectroscopy

Raman spectroscopic micro-analyses were carried out using a Renishaw M1000 micro-Raman spectrometer system. Light from a 514.5 nm argon laser was focused onto the sample with a 100× objective lens, and at 100% power could provide ~5 mW of power at the sample, in a spot size of ~1 µm. Spectral peak positions were calibrated periodically against a silicon standard and rarely varied more than 1 cm^{-1}. All spectra were obtained with a dual-wedge polarization scrambler inserted directly above the objective lens to minimize the effects of polarization. The sample used for the Raman studies was an epoxy-mounted polished grain mount also used for the

electron microprobe analyses. Three spots within a 50 μm × 100 μm joteite region were analysed. On the first spot the laser power was initially adjusted to 10% and worked up to 100% power without any change in the spectrum being recorded. The other two spots at 100% power also gave identical spectra. The spectrum is shown in Fig. 5.

The 1500–100 cm^{-1} region contains the most conspicuous features, a set of prominent composite arsenate ν_1 lines with components at 849 and 861 cm^{-1}. Additional features occur at 725, 506, 461, 414, 384, 283, 162, 140 and 119 cm^{-1}. The 4000–2500 cm^{-1} region of the spectra shows a fairly sharp O–H stretching feature at 3429 cm^{-1} and much broader features centred at 3260, 3068

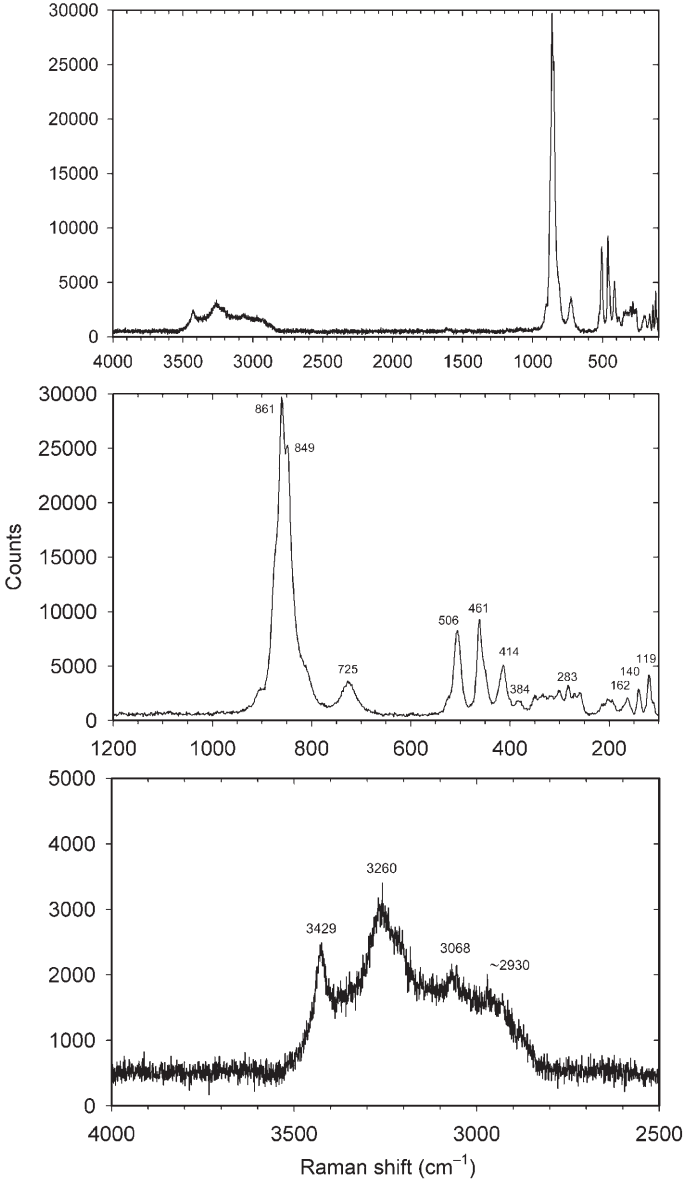

FIG. 5. Raman spectra of joteite: full spectrum (top), expanded view of the 1200 to 100 cm^{-1} region (middle) and expanded view of the 4000 to 2500 cm^{-1} region (bottom).

and ~2930 cm^{-1}. The multitude of O–H features indicates that OH or H_2O occur in multiple environments. The lower-energy features are consistent with hydrogen-bonded, acidic OH groups, such as those in $AsO_3(OH)$ tetrahedra. The absence of bands near 620 cm^{-1} implies that tetrahedral Al species such as $[Al(OH)_4]^-$ or $[AlO(OH)_3]^{2-}$ are not present at significant concentrations (cf. Sipos, 2009).

Special care was taken to check for the possibility of organic contamination that can give Raman signals in the same spectroscopic region. Raman spectra of two crystals on a densely covered matrix and six isolated grains that were scraped off the matrix onto clean Al foil were also obtained. All show the same complex OH-region spectra as the material in the microprobe section, so features in the region that we assign to hydrogen arsenate are not due to contamination from epoxy or other organic materials.

Chemical composition

Five chemical analyses were carried out at the University of Utah on a Cameca SX-50 electron microprobe with four wavelength dispersive spectrometers. Analytical conditions were 15 kV accelerating voltage, 20 nA beam current and a nominal beam diameter of 10–20 μm. Counting times were 10 s for each element. Additional elements sought that were below the limits of detection include Na, Mg, K, Sb, Cl, Mn, Fe and Co. Raw X-ray intensities were corrected for matrix effects with a $\phi(\rho z)$ algorithm (Pouchou and Pichoir, 1991).

No significant beam damage was noted; however, as is typical for highly hydrated phases with loosely held H_2O, joteite dehydrates rapidly under vacuum. Thus, the concentration of the remaining constituents increases with the evolution of H_2O, yielding cation totals greater than expected in the fully hydrated phase. However, the stoichiometric ratios of the cations appear unaffected. Note that the empirical formula (below) indicates a significant excess of Al over that which can be accommodated in the two Al sites in the structure. This is balanced approximately by a deficiency in As. These discrepancies appear to be real, rather than the result of experimental error. We noted the same trend of high Al and low As for other joteite crystals analysed on a JEOL JXA-8200 electron microprobe at the Division of Geological and Planetary Sciences, California Institute of Technology using 15 keV, 5 nA and a 10 μm beam diameter. A structural explanation for the Al excess and As deficiency is considered in the description of the crystal structure below.

Because insufficient material was available for a direct determination of H_2O, the amount of water in joteite was calculated on the basis of 7 total cations, charge balance and 19 O atoms per formula unit (a.p.f.u.), as determined by the crystal structure analysis (see below). Analytical data and standards are given in Table 1. In column 6 of that table, the analytical data are normalized to provide a total of 100 wt.%.

The empirical formula (based on 19 O a.p.f.u.) is $Ca_{1.98}Cu_{1.00}Al_{1.15}As_{2.87}H_{14.24}O_{19}$. The simplified structural formula is $Ca_2CuAl[AsO_4][AsO_3(OH)]_2(OH)_2{\cdot}5H_2O$, which requires CaO 15.72, CuO 11.15, Al_2O_3, 7.14, As_2O_5 48.32, H_2O 17.67, total 100 wt.%. The Gladstone–Dale compatibility index $1 - (K_P/K_C)$ is −0.017 for the ideal formula and −0.019 for the empirical formula, in both cases indicating superior compatibility (Mandarino, 2007).

TABLE 1. Analytical data for joteite.

Constituent	Wt.%	Range	SD	Norm. wt.%	Ideal wt.%	Standard
CaO	17.12	16.54–17.38	0.33	15.70	15.72	Diopside
CuO	12.23	11.13–13.05	0.82	11.22	11.15	Cu metal
Al_2O_3	9.07	9.00–9.15	0.07	8.32	7.14	Syn. YAG
As_2O_5	50.83	48.90–52.38	1.26	46.62	48.32	Syn. GaAs
H_2O*	19.78			18.14	17.67	
Total	109.03			100	100	

* Calculated based on the structure.

X-ray crystallography and structure refinement

Both powder and single-crystal X-ray studies were carried out using a Rigaku R-Axis Rapid II curved imaging plate microdiffractometer, with monochromatized Mo$K\alpha$ radiation. For the powder-diffraction study, observed d spacings and intensities were derived by profile fitting using *JADE 2010* software (Materials Data, Inc.). The powder data presented in Table 2 show good agreement with the pattern calculated from the structure determination. Unit-cell parameters refined from the powder data using *JADE 2010* with whole pattern fitting are: a = 6.044(3), b = 10.220(3), c = 12.898(3) Å, α =

TABLE 2. Powder X-ray data for joteite.

I_{obs}	d_{obs}	d_{calc}	I_{calc}	*hkl*	I_{obs}	d_{obs}	d_{calc}	I_{calc}	*hkl*	I_{obs}	d_{obs}	d_{calc}	I_{calc}	*hkl*
100	12.76	12.6510	100	001			2.6163	1	$0\bar{3}3$			1.7881	1	$\bar{3}\bar{1}2$
7	6.36	6.3255	5	002	3	2.590	2.5950	2	$\bar{2}\bar{2}1$	2	1.780	1.7864	1	036
9	5.77	5.8212	3	100			2.5760	6	$\bar{1}04$			1.7810	1	$0\bar{3}6$
		5.7304	5	101	13	2.501	2.5086	9	040			1.7737	1	$\bar{2}\bar{5}1$
4	5.50	5.5146	3	110			2.5064	4	105			1.7534	3	$2\bar{4}1$
23	5.01	5.0172	19	020			2.4776	2	141	6	1.740	1.7363	1	$3\bar{1}4$
		4.9348	2	$\bar{1}01$			2.4123	2	$\bar{1}\bar{3}3$			1.7277	2	$\bar{1}44$
7	4.70	4.7732	2	102			2.3841	2	$1\bar{1}5$			1.7016	2	$1\bar{4}5$
		4.6625	3	$\bar{1}10$	8	2.375	2.3705	2	$\bar{2}\bar{2}2$			1.6920	1	$0\bar{5}4$
		4.2213	3	120			2.3612	2	$1\bar{3}3$			1.6901	1	$\bar{2}15$
26	4.206	4.2170	14	003			2.3587	2	$2\bar{2}1$	7	1.684	1.6852	1	$1\bar{2}7$
		4.1902	5	121	3	2.305	2.3064	1	$2\bar{2}2$			1.6738	1	$\bar{1}\bar{3}6$
		4.1702	3	$\bar{1}11$			2.3025	4	224			1.6724	2	060
		3.9373	3	022			2.2561	2	$0\bar{2}5$			1.6605	1	227
24	3.920	3.9244	3	$0\bar{2}2$			2.2462	2	$\bar{1}\bar{4}2$	5	1.650	1.6504	1	137
		3.9189	5	$\bar{1}02$	8	2.233	2.2318	3	$\bar{2}21$			1.6490	2	$\bar{2}\bar{4}4$
4	3.780	3.7844	4	103			2.2257	1	143			1.6434	1	$\bar{3}\bar{2}3$
9	3.490	3.5029	4	$\bar{1}12$			2.2190	1	$\bar{2}\bar{1}3$			1.6058	2	$2\bar{4}4$
		3.4846	3	$\bar{1}20$			2.1591	1	043			1.6015	1	118
		3.4627	4	$1\bar{2}1$	6	2.140	2.1528	1	$0\bar{4}3$			1.5968	3	261
25	3.400	3.4006	14	$1\bar{1}3$			2.1325	3	$\bar{2}\bar{2}3$	13	1.596	1.5924	2	$\bar{1}36$
		3.2981	5	$\bar{1}\bar{2}2$			2.1085	3	006			1.5916	1	326
		3.2364	2	031	8	2.110	2.1084	1	234			1.5874	1	260
19	3.233	3.2335	5	023			2.1035	1	$\bar{1}41$			1.5642	1	$1\bar{3}7$
		3.2255	5	123			1.9594	1	$\bar{2}04$	4	1.555	1.5637	1	$2\bar{3}6$
		3.2229	4	$0\bar{2}3$	5	1.950	1.9404	1	300			1.5564	1	063
		3.0833	4	$\bar{1}\bar{1}3$			1.9390	1	320			1.5528	1	$0\bar{6}3$
		3.0194	2	014			1.9101	1	303			1.4895	2	354
		3.0025	2	$\bar{1}31$	6	1.910	1.9100	1	323			1.4892	1	$3\bar{3}4$
20	2.970	2.9711	3	132			1.9042	1	216	8	1.485	1.4856	1	264
		2.9659	9	201			1.8922	1	206			1.4830	1	402
15	2.910	2.9142	5	$\bar{1}22$			1.8571	2	$\bar{1}\bar{1}6$			1.4789	1	401
		2.9112	9	$\bar{1}13$	5	1.857	1.8526	1	136			1.4584	1	$\bar{1}6\bar{4}$
		2.8515	4	$1\bar{2}3$			1.8508	2	314			1.4571	1	$\bar{2}44$
11	2.811	2.8289	3	$1\bar{1}4$			1.8211	1	117			1.4542	1	$\bar{3}\bar{5}2$
		2.8054	12	221			1.8183	1	$\bar{1}16$	6	1.451	1.4500	1	$\bar{1}\bar{1}8$
		2.7573	2	220	2	1.815	1.8177	1	$2\bar{1}6$			1.4498	1	165
		2.7203	2	$\bar{1}\bar{3}2$			1.8145	1	053			1.4422	1	$\bar{1}37$
		2.6863	1	$\bar{1}30$			1.8137	1	252					
3	2.680	2.6817	3	133			1.8109	1	$2\bar{3}4$					
		2.6796	1	024										

Only calculated lines with intensities greater than 1 are listed unless they correspond to observed lines.

87.413(19), β = 78.463(15), γ = 78.789(18)º and V = 765.6(4) Å^3.

Structure data were collected using a total of 152 frames at 25-min exposures. The *Rigaku CrystalClear* software package was used for processing the structure data, including the application of an empirical absorption correction. The *TwinSolve* program in the *CrystalClear* software package readily showed the reflections to be from two twin domains of essentially equal intensity and determined the twinning to be by reflection on {001}. The reflections in both domains were then integrated using *TwinSolve* to create a SHELX HKLF5 file. The structure was solved by direct methods using *SHELXS* and was refined using *SHELXL* (Sheldrick, 2008). The relatively high R factor is attributed to the small size and marginal quality of the crystal and the imperfect nature of refinement using a dataset obtained from a twinned crystal. The data collection and structure refinement details are provided in Table 3, atom coordinates and displacement parameters in Table 4, selected bond distances in Table 5 and bond valence summations in Table 6. Lists of observed and calculated structure factors have been deposited with the the Principal Editor of *Mineralogical Magazine* and can be downloaded from http://www.minersoc.org/pages/e_journals/dep_mat_mm.html.

Description of the structure

In the structure of joteite (Fig. 6), AsO_4 and $AsO_3(OH)$ tetrahedra, $AlO_4(OH)_2$ octahedra and $Cu^{2+}O_2(OH)_2(H_2O)$ square pyramids share

TABLE 3. Data collection and structure refinement details for joteite.

Diffractometer	Rigaku R-Axis Rapid II
X-ray radiation/power	Mo$K\alpha$ (λ = 0.71075 Å)/50 kV, 40 mA
Temperature	298(2) K
Ideal Formula	$Ca_2CuAl[AsO_4][AsO_3(OH)]_2(OH)_2{\cdot}5H_2O$
Space group	$P\bar{1}$
Unit-cell dimensions	a = 6.0530(2) Å
	b = 10.2329(3) Å
	c = 12.9112(4) Å
	α = 87.572(2)º
	β = 78.480(2)º
	γ = 78.697(2)º
V	768.40(4) Å^3
Z	2
Density (for above formula)	3.084 g cm^{-3}
Absorption coefficient	8.661 mm^{-1}
F(000)	694
Crystal size (μm)	80 × 50 × 5
θ range	2.03 to 30.07º
Index ranges	$0 \leqslant h \leqslant 8$, $-13 \leqslant k \leqslant 14$, $-17 \leqslant l \leqslant 18$
Reflections collected/unique	8440 / 8440
Reflections with $F > 4\sigma(F)$	6003
Completeness to θ = 30.07º	99.0%
Max. and min. transmission	0.9580 and 0.5441
Refinement method	Full-matrix least-squares on F^2
Parameters refined	240
GoF	1.106
Final R indices [$F_o > 4\sigma(F)$]	R_1 = 0.0772, wR_2 = 0.2053
R indices (all data)	R_1 = 0.1167, wR_2 = 0.2200
Extinction coefficient	0.0047(16)
Largest diff. peak / hole	+2.396 / −2.324 e A^{-3}

$R_{int} = \Sigma|F_o^2\text{-}F_o^2(\text{mean})|/\Sigma[F_o^2]$. GoF = $S = \{\Sigma[w(F_o^2-F_c^2)^2]/(n-p)\}^{1/2}$. $R_1 = \Sigma||F_o|\text{-}|F_c||/\Sigma|F_o|$. $wR_2 = \{\Sigma[w(F_o^2-F_c^2)^2]/\Sigma[w(F_o^2)^2]\}^{1/2}$. $w = 1/[\sigma^2(F_o^2) + (aP)^2 + bP]$ where a is 0.1038, b is 7.6497 and P is $[2F_c^2 + \text{Max}(F_o^2,0)]/3$.

TABLE 4. Atom coordinates and displacement parameters (Å^2) for joteite.

	x/*a*	*y*/*b*	*z*/*c*	U_{eq}	U_{11}	U_{22}	U_{33}	U_{23}	U_{13}	U_{12}
Ca1	0.1927(3)	0.93935(18)	0.81685(15)	0.0097(4)	0.0130(8)	0.0086(8)	0.0097(9)	0.0026(6)	–0.0049(7)	–0.0049(7)
Ca2	0.4829(3)	0.54746(18)	0.82364(15)	0.0103(4)	0.0116(8)	0.0085(8)	0.0103(9)	–0.0014(6)	0.0011(6)	–0.0037(7)
Cu	0.31806(18)	0.24809(11)	0.85644(9)	0.0067(2)	0.0045(4)	0.0036(4)	0.0123(5)	0.0007(4)	–0.0023(4)	–0.0008(4)
Al1	0.5000	0.0000	0.0000	0.0049(7)	0.0061(16)	0.0037(16)	0.0050(17)	0.0009(12)	–0.0006(13)	–0.0018(13)
Al2	0.0000	0.5000	0.0000	0.0033(6)	0.0052(15)	0.0015(15)	0.0030(16)	–0.0003(12)	–0.0012(12)	0.0007(12)
As1	0.78742(14)	0.24612(9)	0.93661(7)	0.00466(19)	0.0053(4)	0.0035(4)	0.0059(4)	–0.0001(3)	–0.0016(3)	–0.0021(3)
As2	0.78581(15)	0.75022(9)	0.86052(7)	0.0067(2)	0.0084(4)	0.0050(4)	0.0068(4)	0.0008(3)	–0.0023(3)	–0.0013(3)
As3	0.05410(16)	0.25036(10)	0.49586(7)	0.0101(2)	0.0111(4)	0.0114(4)	0.0074(4)	–0.0005(3)	–0.0019(3)	–0.0010(3)
O1	0.5949(11)	0.3163(6)	0.8631(5)	0.0086(12)	0.012(3)	0.008(3)	0.008(3)	0.007(2)	–0.004(2)	–0.005(2)
O2	0.0375(11)	0.1788(7)	0.8575(5)	0.0116(13)	0.010(3)	0.015(3)	0.012(3)	–0.002(3)	–0.004(2)	–0.004(3)
O3	0.6930(10)	0.1246(6)	0.0153(5)	0.0080(12)	0.009(3)	0.003(3)	0.012(3)	0.000(2)	0.000(2)	–0.004(2)
O4	0.1874(10)	0.6356(6)	0.9816(5)	0.0091(12)	0.007(3)	0.010(3)	0.010(3)	–0.002(2)	0.000(2)	–0.002(2)
O5	0.5812(11)	0.7642(6)	0.7898(5)	0.0082(12)	0.012(3)	0.002(3)	0.012(3)	0.000(2)	–0.006(2)	–0.004(2)
O6	0.7751(11)	0.8800(6)	0.9387(5)	0.0084(12)	0.008(3)	0.007(3)	0.013(3)	0.000(2)	–0.007(2)	–0.001(2)
O7	0.7713(10)	0.6074(6)	0.9327(5)	0.0072(11)	0.008(3)	0.005(3)	0.009(3)	0.003(2)	–0.003(2)	–0.002(2)
OH8	0.0545(11)	0.7398(7)	0.7814(5)	0.0103(12)	0.016(3)	0.013(3)	0.003(3)	0.003(2)	0.002(2)	–0.009(3)
O9	0.1992(13)	0.0992(7)	0.4613(6)	0.0175(15)	0.018(4)	0.016(4)	0.016(4)	–0.006(3)	–0.002(3)	0.003(3)
O10	0.8745(12)	0.2564(8)	0.6118(6)	0.0176(15)	0.016(3)	0.018(3)	0.014(4)	0.002(3)	0.005(3)	–0.002(3)
O11	0.9259(13)	0.3284(7)	0.4006(6)	0.0184(15)	0.020(4)	0.017(4)	0.017(4)	–0.005(3)	–0.010(3)	0.008(3)
OH12	0.2399(14)	0.3579(8)	0.5077(6)	0.0222(17)	0.028(4)	0.021(4)	0.023(4)	–0.001(3)	–0.005(3)	–0.019(3)
OH13	0.4666(10)	0.0615(6)	0.8632(5)	0.0063(12)	0.007(3)	0.003(3)	0.011(3)	–0.002(2)	–0.005(2)	–0.002(2)
OH14	0.1610(10)	0.4325(6)	0.8657(5)	0.0053(11)	0.005(3)	0.006(3)	0.006(3)	0.000(2)	–0.003(2)	0.000(2)
OW15	0.4267(11)	0.2394(7)	0.6676(6)	0.0150(14)	0.011(3)	0.017(3)	0.021(4)	0.002(3)	–0.008(3)	–0.006(3)
OW16	0.8802(12)	0.4721(7)	0.7208(6)	0.0136(14)	0.014(3)	0.010(3)	0.017(4)	–0.003(3)	–0.001(3)	–0.005(3)
OW17	0.3668(13)	0.9723(8)	0.6373(6)	0.0187(15)	0.016(3)	0.028(4)	0.010(4)	–0.006(3)	–0.001(3)	0.001(3)
OW18	0.4599(13)	0.5299(8)	0.6440(6)	0.0216(16)	0.016(4)	0.031(4)	0.016(4)	–0.005(3)	–0.003(3)	–0.002(3)
OW19	0.8797(12)	0.0183(7)	0.7161(6)	0.0129(14)	0.018(3)	0.008(3)	0.012(3)	0.008(2)	–0.002(3)	–0.004(3)

TABLE 5. Selected bond distances (Å) in joteite.

Ca1–OW17	2.386(8)	Al1–OH13(×2)	1.886(6)	Hydrogen bonds	
Ca1–O3	2.430(7)	Al1–O6(×2)	1.913(6)	OH8–O11	2.454(10)
Ca1–OH13	2.438(6)	Al1–O3(×2)	1.931(6)	OH12–OW15	2.682(11)
Ca1–OH8	2.445(7)	<Al1–O>	1.910	OH13–OW19	2.792(9)
Ca1–O2	2.484(7)			OH14–O7	2.717(8)
Ca1–OW19	2.495(7)	Al2–OH14(×2)	1.896(6)	OW15–O10	2.700(10)
Ca1–O5	2.634(7)	Al2–O7(×2)	1.919(6)	OW15–OW17	2.879(11)
Ca1–O6	2.858(7)	Al2–O4(×2)	1.937(6)	OW16–O10	2.677(10)
<Ca1–O>	2.521	<Al2–O>	1.917	OW16–O11	2.818(10)
				OW17–O9	2.655(11)
Ca2–OW18	2.368(8)	As1–O1	1.682(6)	OW17–O9	2.835(11)
Ca2–O1	2.392(7)	As1–O2	1.686(7)	OW18–O11	2.651(11)
Ca2–O5	2.407(6)	As1–O3	1.686(6)	OW18–OH12	2.768(10)
Ca2–OH14	2.428(6)	As1–O4	1.688(6)	OW19–O9	2.795(10)
Ca2–OW16	2.495(7)	<As1–O>	1.686	OW19–O10	2.732(10)
Ca2–O4	2.498(7)				
Ca2–O7	2.623(6)	As2–O5	1.661(6)		
Ca2–OH8	3.061(7)	As2–O6	1.686(6)		
<Ca1–O>	2.459	As2–O7	1.707(6)		
		As2–OH8	1.726(6)		
Cu–OH14	1.936(6)	<As2–O>	1.695		
Cu–OH13	1.951(6)				
Cu–O1	1.955(6)	As3–O9	1.653(7)		
Cu–O2	1.962(6)	As3–O10	1.660(7)		
Cu–OW15	2.396(8)	As3–O11	1.675(7)		
<Cu–O>	2.040	As3–OH12	1.751(7)		
		<As3–O>	1.685		

corners to form sheets parallel to {001} (Fig. 7). In addition, 7- and 8-coordinate Ca polyhedra, $CaO_5(H_2O)_2$ and $CaO_5(OH)(H_2O)_2$, link to the periphery of the sheets by corner and edge sharing to create thick slabs. Between the slabs are isolated (unconnected) $AsO_3(OH)$ tetrahedra, which link the slabs only via hydrogen bonding (Fig. 8). The perfect cleavage and ubiquitous twinning, both on {001}, are clearly related to the weak bonding across this interlayer region.

The structure is not closely related to that of any other mineral. One of the more interesting features of the structure is the unconnected $AsO_3(OH)$ tetrahedron, which is rare in arsenate (and phosphate) structures. Among the mineral structures with unconnected arsenate or phosphate groups are those of the arsenate rösslerite (Ferraris and Franchini-Angela, 1973) and the phosphates phosphorrösslerite (Street and Whitaker, 1973) and struvite (Ferraris *et al*., 1986). In the structures of rösslerite, phosphorrösslerite and struvite, the unconnected tetrahedral group is also an acid arsenate or phosphate; however, the only other structural component in these structures is an isolated $Mg(H_2O)_6$ octahedron. Structures with isolated sulfate tetrahedra are much more common and include many mineral groups such as the hexahydrite, epsomite, melanterite, picromerite, ettringite and fleischerite groups (Hawthorne *et al*., 2000). The key to the stability of the unconnected acid arsenate or phosphate group is an extensive network of hydrogen bonds to the O atoms of the group to achieve bond-valence balance. The hydrogen bonding involving the unconnected $AsO_3(OH)$ group in the joteite structure is shown in Fig. 8 and bond-valence balance (Table 6) for the O9, O10, O11 and OH12 atoms of the group is seen to be quite effectively achieved: 1.93, 1.95, 2.07 and 2.02 v.u., respectively.

Finally, some comments on the Al excess and As deficiency in the empirical formula from a structural perspective seem warranted. Al^{3+} does not typically substitute for As^{5+} in tetrahedral coordination, probably because of the very different charges and electronegativities of these cations. Nevertheless, we must consider the possibility that Al replaces some of the As in

TABLE 6. Bond-valence analysis for joteite. Values are expressed in valence units.

	O1	O2	O3	O4	O5	O6	O7	OH8	O9	O10	O11	OH12	OH13	OH14	OW15	OW16	OW17	OW18	OW19	Sum
Ca1		0.25	0.29		0.16	0.09		0.27					0.28				0.32		0.24	1.90
Ca2	0.32			0.24	0.30		0.17							0.29		0.24		0.34		1.90
Al1			0.47 ×2→			0.49 ×2→							0.53 ×2→							2.98
Al2				0.46 ×2→			0.48 ×2→							0.52 ×2→						2.92
Cu	0.47	0.47											0.48	0.50	0.14					2.06
As1	1.26	1.24	1.24	1.24																4.98
As2					1.33	1.24	1.18	1.12												4.87
As3									1.36	1.34	1.28	1.04								5.02
H8								0.61			0.39									1.00
H12												0.79			0.21					1.00
H13													0.82						0.18	1.00
H14							0.20							0.80						1.00
H15a										0.20					0.80					1.00
H15b															0.84		0.16			1.00
H16a										0.21						0.79				1.00
H16b											0.18					0.82				1.00
H17a									0.22								0.78			1.00
H17b									0.17								0.83			1.00
H18a											0.22							0.78		1.00
H18b												0.19						0.81		1.00
H19a									0.18										0.82	1.00
H19b										0.20									0.80	1.00
Sum	2.05	1.96	2.00	1.94	1.80	1.83	2.03	2.00	1.93	1.95	2.07	2.02	2.11	2.10	1.99	1.85	2.09	1.93	2.04	

Multiplicity is indicated by ×→; bond strengths from Brown and Altermatt (1985); hydrogen-bond strengths based on O···O bond lengths, also from Brown and Altermatt (1985).

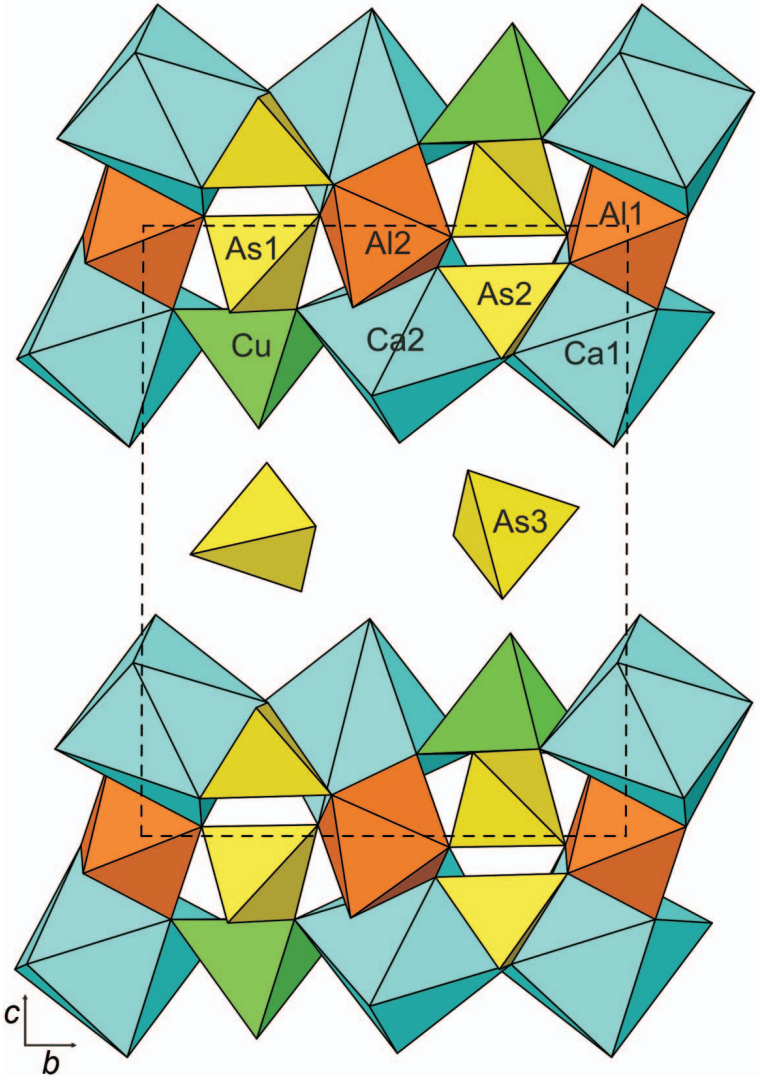

FIG. 6. Structure of joteite showing the unconnected $AsO_3(OH)$ in the interlayer.

the structure. The most likely As site to be involved is As3 because of the isolated, 'flexible' placement of the $As3O_3(OH)$ group in the interlayer region and the fact that the equivalent isotropic displacement parameters (U_{eq}) for the As3 site and the surrounding arsenate O sites are significantly higher than those for these sites in the other arsenate groups. There is no obvious vacant site in the Cu-Al-Ca layer that could accommodate additional Al. To allow the Al and As contents indicated by the EMPA, ~15% of the As in the As3 site would need to be replaced by Al. The simplest substitution mechanism would be for the $[AsO_3(OH)]^{2-}$ tetrahedron to be replaced by $[AlO(OH)_3]^{2-}$. Refining the As3 site with joint occupancy with both As and Al, provides <2% occupancy by Al and leaves U_{eq} still significantly higher than those of the other As sites, while setting the site occupancy to 85% As and 15% Al brings U_{eq} into line with those of the other As sites, but increases R_1 from 7.72% to 7.91%. We note above that the Raman spectrum shows no evidence of tetrahedral Al in the structure, so it is possible that any additional

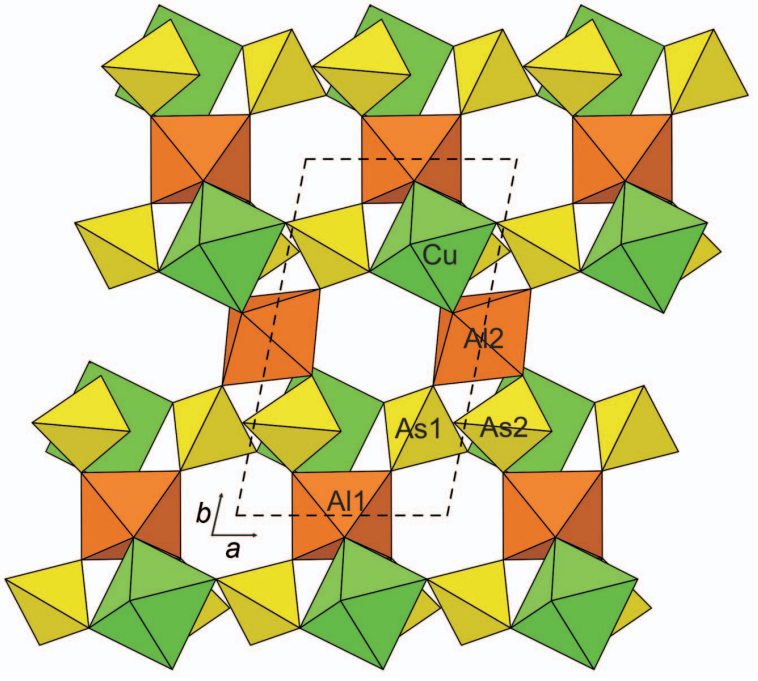

FIG. 7. Sheet of corner-sharing AsO_4 and $AsO_3(OH)$ tetrahedra, AlO_6 octahedra and $Cu^{2+}O_5$ square pyramids in the structure of joteite.

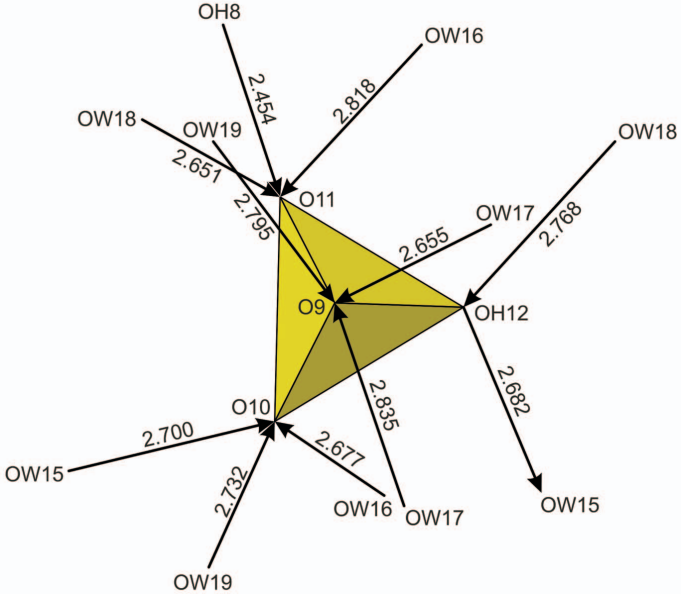

FIG. 8. Hydrogen bonds to and from the interlayer $AsO_3(OH)$ tetrahedron (As3). The arrows point in the direction of the acceptor O atoms.

interlayer Al is octahedrally coordinated, and present as an anion such as $[Al(OH)_5(H_2O)]^{2-}$ rather than tetrahedral $[AlO(OH)_3]^{2-}$. The octahedral species would be expected to produce Raman bands near 490–500 cm^{-1} (Watling *et al*., 1999), along with the other AlO_6 octahedra of the structure (cf. Fig. 5). An interlayer octahedron would participate in the hydrogen bond network differently from a tetrahedron, and hence would be unlikely to have its centroid at the same place. A 15% occupied Al site may account for the largest residual electron density peak of 1.70 electrons near As3 at [−0.2371, −0.2501, 0.9334]. The low occupancy of the associated oxygen sites, and the accompanying small increase in H_2O content, would be challenging to verify experimentally given the quality of the crystals. In the end, we are forced to conclude that the structure refinement does not provide unambiguous evidence to explain the Al excess and As deficiency in the empirical formula or the structural mechanism of the substitution.

Acknowledgements

Andrew Christy, Joel Grice and Fernando Cámara are thanked for their constructive comments on the manuscript. Arturo Molina is thanked for providing specimens of joteite. Work at the California Institute of Technology was supported by NSF grant EAR-0947956 and a grant from the Northern California Mineralogical Association. The remainder of this study was funded by the John Jago Trelawney Endowment to the Mineral Sciences Department of the Natural History Museum of Los Angeles County.

References

Brown, I.D. and Altermatt, D. (1985) Bond-valence parameters from a systematic analysis of the inorganic crystal structure database. *Acta Crystallographica*, **B41**, 244–247.

Ferraris, G. and Franchini-Angela, M. (1973) Hydrogen bonding in the crystalline state. Crystal structure of $MgHAsO_4 \cdot 7H_2O$ roesslerite. *Acta Crystallographica*, **B29**, 286–292.

Ferraris, G., Fuess, H. and Joswig, W. (1986) Neutron diffraction study of $MgNH_4PO_4(H_2O)_6$ (struvite) and survey of water molecules donating short hydrogen bonds. *Acta Crystallographica*, **B42**, 253–258.

Hawthorne, F.C., Krivovichev, S.V. and Burns, P.C. (2000) The crystal chemistry of sulfate minerals. Pp. 1–112 in: *Sulfate Minerals – Crystallography, Geochemistry, and Environmental Signifcance*. Reviews in Mineralogy, **40**. Mineralogical Society of America, Washington, D.C.

Kampf, A.R. (2009) Miguelromeroite, the Mn analogue of sainfeldite, and redefinition of villyaellenite as an ordered intermediate in the sainfeldite-miguelromeroite series. *American Mineralogist*, **94**, 1535–1540.

Mandarino, J.A. (2007) The Gladstone–Dale compatibility of minerals and its use in selecting mineral species for further study. *The Canadian Mineralogist*, **45**, 1307–1324.

Parker, R.L., Salas, R.O. and Perez, G.R. (1963) Geologia de los distritos mineros Checo de Cobre Pampa Larga y Cabeza de Vaca. *Instituto de Investigaciones Geologicas*, **14**, 40–42.

Popova, V.I., Popov, V.A., Clark, A. Polyakov, V.O. and Borisovskii, S.E. (1986) Alacranite – a new mineral. *Zapiski Vsesoyuznogo Mineralogicheskogo Obshchestva*, **115**, 360–368 (in Russian).

Pouchou, J.-L. and Pichoir, F. (1991) Quantitative analysis of homogeneous or stratified microvolumes applying the model "PAP." Pp. 31–75 in: *Electron Probe Quantitation* (K.F.J. Heinrich and D.E. Newbury, editors). Plenum Press, New York.

Sheldrick, G.M. (2008) A short history of *SHELX*. *Acta Crystallographica*, **A64**, 112–122.

Sipos, P. (2009) The structure of Al(III) in strongly alkaline aluminate solutions – a review. *Journal of Molecular Liquids*, **146**, 1–14.

Street, R.L.T. and Whitaker, A. (1973) The isostructurality of rosslerite and phosphorosslerite. *Zeitschrift für Kristallographie*, **137**, 246–255.

Watling, H.R., Sipos, P.M., Byrne, L., Hefter, G.T. and May, P.M. (1999) Raman, IR, and Al-27 MAS NMR spectroscopic studies of sodium (hydroxy)aluminates. *Applied Spectroscopy*, **53**, 415–422.

Yang, H., Jenkins, R.A., Downs, R.T., Evans, S.H. and Tait, K.T. (2011) Rruffite, $Ca_2Cu(AsO_4)_2 \cdot 2H_2O$, a new member of the roselite group, from Tierra Amarilla, Chile. *The Canadian Mineralogist*, **49**, 877–884.